Improved Amplified Spontaneous Emission of Dye-Doped Functionalized Mesostructured Silica Waveguide Films

Manuel G. Ramírez, Justin P. Jahnke, Matthias J. N. Junk, José M. Villalvilla, Pedro G. Boj, José A. Quintana, Eva M. Calzado, Bradley F. Chmelka, and María A. Díaz-García**

Amplified spontaneous emission (ASE) in dye-doped mesostructured silica films, deposited directly over fused silica substrates, is demonstrated with low thresholds. Due to functionalization of the silica network with phenyl groups, the refractive index of the active layer is sufficiently increased to impart waveguiding properties that lead to highly efficient ASE. Such functionalization eliminates the need for a separate low-refractive-index layer between the active film and the substrate, as is often used to achieve waveguiding properties with silica mesostructured materials, though which is typically accompanied by significant optical losses that reduce overall ASE performance. By forming a high-quality waveguide without the need for a separate low-refractive-index layer, significantly improved properties are obtained, with ASE thresholds as low as 8 kW cm^{-2}. Solid-state 2D NMR spectroscopy measurements establish the compositions and structures of the active mesostructured film at a molecular level, in particular that phenyl functionalization of the mesochannel surfaces promotes the homogeneous dispersion of the laser dye species over nanoscale dimensions in the materials.

1. Introduction

Organic solid-state lasers with active materials prepared as waveguide films have been intensively investigated over the past two decades for applications in the fields of optical communications,[1] biosensing, and chemical sensing.[2,3] A wide variety of materials have been used to form active waveguide films,[4] including laser dyes dispersed in inert matrices, nondiluted films of semiconducting materials (e.g., polymers, oligomers, dendrimers, or small molecules), and very recently also single crystals. Within the subclass of dye-doped systems, the use of mesostructured materials as matrices into which the laser dyes are dispersed[5] constitutes a very promising approach. Such mesostructured materials offer the possibility of controlling dye locations and orientations within the matrix. Both factors significantly influence the film photoluminescence (PL) efficiency and consequently the final laser performance.[6]

Mesostructured materials have received great attention in numerous scientific and technological areas, including catalysis; electronic, optoelectronic, and photovoltaic devices; and chemical and biological sensors.[7] These materials are facilely prepared from solution by coassembly and cross-linking of network-forming inorganic species, typically oxides such as silica or titania, in the presence of structure-directing organic agents, typically amphiphilic surfactants or block copolymers.[8] Depending on the initial solution composition and processing conditions, a wide range of highly ordered mesoscale (2–50 nm) morphologies (e.g., cubic, hexagonal, lamellar) can be formed. These materials can easily be processed to form fibers, films, or monoliths, enabling their integration in diverse technological devices.[9] The surfactant properties of the block copolymer species enable the incorporation of high concentrations of photoresponsive guest species, such as laser dyes, for optoelectronic applications. In addition, these materials can be prepared with a high degree of macroscopic ordering. Such order may potentially be exploited to obtain anisotropic optical properties that can be very useful in the case of large organic molecules or polymers.[10]

Because of their numerous potential advantages, dye-doped mesostructured silica films have previously been investigated as

Dr. M. G. Ramírez, Dr. J. M. Villalvilla,
Prof. M. A. Díaz García
Dpto. Física Aplicada
Instituto Universitario de Materiales de Alicante (IUMA)
y Unidad Asociada UA-CSIC
Universidad de Alicante
Alicante 03080, Spain
E-mail: maria.diaz@ua.es
Dr. J. P. Jahnke, Dr. M. J. N. Junk, Prof. B. F. Chmelka
Department of Chemical Engineering
University of California
Santa Barbara, CA 93106, USA
E-mail: bradc@engineering.ucsb.edu
Dr. P. G. Boj, Dr. J. A. Quintana
Dpto. Óptica
IUMA y Unidad Asociada UA-CSIC
Universidad de Alicante
Alicante 03080, Spain
Dr. E. M. Calzado
Dpto. Física
Ingeniería de sistemas y teoría de la señal and IUMA
Universidad de Alicante
Alicante 03080, Spain

DOI: 10.1002/adom.201500297

active laser materials in waveguide-based devices.[5a,b] To enable waveguiding in the active dye-doped mesostructured silica film, its refractive index (n_f) should be larger than that of the substrate (n_s). Since n_f of mesostructured films is between 1.4 and 1.5, similar to that of the fused silica substrate, a low refractive index (n) cladding layer, typically mesoporous SiO_2 with $n \approx 1.2$, was intercalated between the active film and the substrate in previous studies.[5a,c] The need to employ such low-n layers constitutes an important limitation, given the poor stability and optical quality of the mesoporous silica materials normally used for that purpose. Therefore, design strategies to avoid the use of such layers is of great interest to simplify device fabrication and, more importantly, to improve their lasing properties.

The easiest way to assess the potential of a given material for a waveguide-based laser device is to study its amplified spontaneous emission (ASE) properties when deposited as a thin film in a waveguide configuration.[4a–c] ASE is evidenced by a collapse of the width of the PL spectrum and a large enhancement of the output intensity at a certain optical pump intensity, the ASE threshold. This indicates the presence of optical gain due to stimulated emission. For a good ASE performance, a low-loss waveguide film with high PL efficiency is required. Both aspects are highly dependent on the type of laser dye, host matrix, and substrate material, as well as on parameters such as the dye-doping ratio,[6] the film thickness,[11] and the refractive index difference between the film and the substrate.[11b,12] Therefore, proper material selection and parameter adjustments are crucial to optimize the active medium before its inclusion in the laser cavity.

Rhodamine 6G (Rh6G) was employed as laser dye in many previous studies with mesostructured materials.[5] In recent years, perylenediimides (PDIs) have shown much better ASE and laser performances, e.g., excellent photostabilities and lower thresholds than Rh6G and other dyes in various types of devices.[6,13,14] PDIs are highly stable organic molecules displaying a large substituent-dependent absorption in the 450–600 nm region, as well as a bright fluorescence with quantum yields close to unity.[15] The derivative denoted as perylene orange (PDI-O, see chemical structure in **Figure 1**a), with 2,6-diisopropylphenyl groups attached at the imide positions, has been to date the PDI compound showing the lowest ASE threshold (around 3 kW cm^{-2}), particularly when dispersed into thermoplastic polymers, such as polystyrene (PS) or poly(methyl methacrylate) (PMMA), at concentrations between 0.5 and 3 wt%.[6b]

In the present work, we report ASE in PDI-O-doped mesostructured silica films, deposited directly over fused silica substrates. In contrast to previous laser studies with mesostructured silica-based materials, a low refractive index cladding layer intercalated between the active film and the substrate is not needed to obtain ASE. This was accomplished by functionalizing the mesostructured silica network with phenyl groups (Figure 1b). The phenyl groups increase the refractive index of the active layer sufficiently to allow the formation of waveguides and to enable ASE at low thresholds. Small-angle X-ray scattering was used to establish the presence of mesostructural order in the phenyl-functionalized silica films. The location and degree of dispersion of the laser dye within the silica matrix was inferred by solid-state 2D NMR experiments.

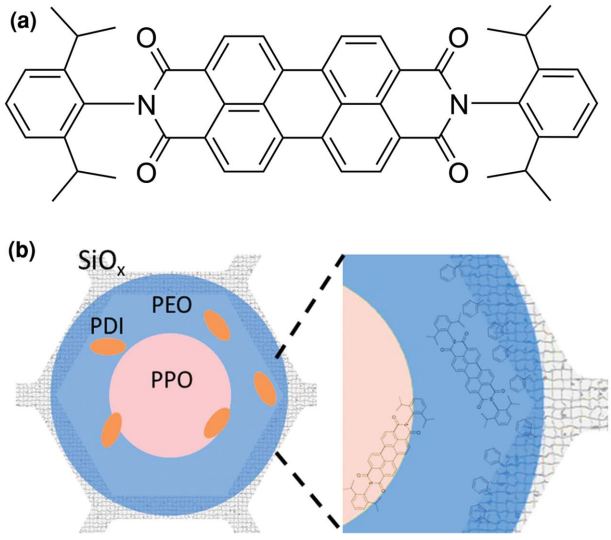

Figure 1. Chemical structure of a) PDI-O and b) silica functionalized with phenyl groups [$Si(Ph)_xO_{2-0.5x}$]. PPO: poly(propyleneoxide); PEO: poly(ethyleneoxide).

2. Results and Discussion

2.1. Synthesis, Waveguide Fabrication, and Structural Characterization

Films of standard, nonfunctionalized, and phenyl-functionalized mesostructured silica doped with the laser dye PDI-O were deposited over commercial fused silica plates by spin-coating. The nonfunctionalized silica was synthesized according to previously reported methods from solutions containing tetraethoxysilane (TEOS) and the structure-directing surfactant triblock copolymer Pluronic P123 (see the Experimental Section for details). To prepare phenyl-functionalized mesostructured silica, triethoxyphenylsilane ($SiPh(OEt)_3$) was added in various proportions to the initial solution containing TEOS. Films with TEOS:$SiPh(OEt)_3$ weight ratios of 10:1, 10:3, and 10:6 were prepared. This notation will be used to account for the degree of functionalization. In all cases, the PDI-O laser dye was added in the final step of the synthesis to the solution containing either TEOS/P123 or TEOS/$SiPh(OEt)_3$/P123. The amount of PDI-O, expressed as a percentage with respect to the expected final film mass (i.e., the mass of P123 plus fully condensed silica), was varied from 0.5% to 3%. The films were prepared over either mesoporous SiO_2 layers of low refractive index (n = 1.2), or directly on fused silica plates, as discussed in the Experimental Section.

The presence of mesostructural order in the surfactant-directed nonfunctionalized and phenyl-functionalized mesostructured silica films with 2% PDI-O incorporated is established by small-angle X-ray scattering (SAXS, **Figure 2**). X-ray scattering is sensitive to long-range periodicities of electron density, which can be related to the periodic order within the block copolymer mesostructured composites. For example, Figure 2a shows the SAXS pattern obtained for a P123-directed

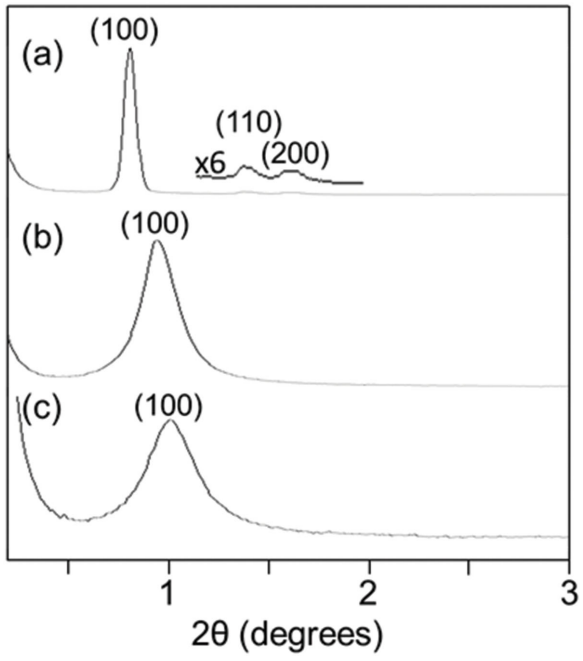

Figure 2. Small-angle X-ray scattering patterns of P123-directed mesostructured films with 2% PDI-O and either a) an SiO_2 framework, b) a 10:3 SiO_2:$SiO_{1.5}$(phenyl) framework, or c) a 10:6 SiO_2:$SiO_{1.5}$(phenyl) framework. The position of the characteristic (100) reflection changes to higher angles upon phenyl functionalization and the secondary (110) and (200) reflections disappear.

mesostructured silica film synthesized without phenyl functionalization. Three reflections are observed at 0.81°, 1.4°, and 1.6°, which correspond to *d*-spacings of 11.0, 6.3 and 5.5 nm, respectively, and which can be assigned as the (100), (110), and (200) reflections of a well-ordered hexagonal structure.[16] In a P123-directed film with a 10:3 SiO_2:$SiO_{1.5}$(phenyl) ratio (Figure 2b), a single, broader reflection is observed at 0.94°, which corresponds to a *d*-spacing of 9.3 nm. This broadening and shift to smaller *d*-spacings reflects a less ordered structure due to the presence of phenyl surface functionalization. This trend toward broader reflections at larger angles is confirmed by a SAXS pattern acquired for a P123-directed film with a 10:6 SiO_2:$SiO_{1.5}$(phenyl) ratio (Figure 2c). Specifically, a single broad reflection is observed at 1.0°, which corresponds to a *d*-spacing of 8.8 nm and demonstrates that even at this high surface phenyl concentration, a mesostructurally ordered material is obtained. The SAXS measurements establish that mesostructurally ordered P123-silica films can be synthesized with a range of surface phenyl functionalizations up to 10:6. A higher extent of phenyl functionalization would further decrease the mesostructural order and thereby diminish the advantage of these materials as matrixes to disperse the laser dyes. Efforts to prepare films with higher functionalization ratios resulted in films that exhibited poor optical properties. The decrease of the optical quality of the films upon functionalization is supported by the different relative percentages of diffused light intensity measured, specifically 6%, 30%, and >80% for functionalization ratios of 10:1, 10:3, and 10:6, respectively.

2.2. Optical Properties of the Films: Absorption, Photoluminescence, and Amplified Spontaneous Emission

One key property to optimize the active laser material performance is the dye concentration in the matrix. Generally, it is desirable to increase it as much as possible to increase PL efficiency, and thereby obtain a lower ASE threshold. However, there is a limiting concentration at which the existence of molecular interactions and/or the formation of aggregated species leads to PL quenching and subsequent saturation that often lead to an increase of the ASE threshold.[6] Information about this limiting concentration can indirectly be obtained from changes in the absorption (ABS) and/or PL spectral shape. For example, in previous studies of PDI-doped PS, aggregation of the PDI derivatives gave rise to changes of the PL spectral shape. The intensity of the 0–1 vibrational peak increased relative to that of the 0–0 main transition. On the other hand, the shape of the ABS spectra remained unchanged despite PDI aggregation.[6a,b] For the PDI-O derivative used in the present work, saturation of the PL film intensity started at concentrations of around 3 wt%.[6b]

In order to explore this issue in our materials, nonfunctionalized mesostructured films with PDI-O contents between 0.5% and 3.5% were prepared over fused silica plates and their ABS and PL spectra were measured (see the Supporting Information, Figure S1). In contrast to results reported for PS-dispersed PDI-O, the presence of molecular interactions manifests in changes of the ABS spectra. For PDI-O contents of 0.5% and below, the shapes of the ABS spectra are similar to those of PDI-O in liquid solution or dispersed in PS. For PDI-O concentrations above 0.5%, a new absorption band appears at 544 nm, which is indicative of the formation of aggregated species. Although the PL spectral shapes are similar for all concentrations, strong PL quenching occurs when the concentration increases from 0.5 to 1.5% and above. In view of these results a doping ratio of 0.5% PDI-O was chosen for the phenyl-functionalized silica films to be used for the ASE studies.

Absorption and PL spectra of 0.5% PDI-O-doped phenyl-functionalized silica films had similar shapes to those of otherwise identical nonfunctionalized silica films when the degree of phenyl functionalization was varied from 10:1 to 10:6. Slight redshifts of a few nanometers, attributed to changes in the local chemical environment, were observed upon functionalization (see **Figure 3**a). Spectral narrowing due to ASE was only observed for 10:3 and 10:6 phenyl-functionalized films. The corresponding spectra are included in Figure 3a. As a consequence of the slight redshift of the PL spectrum upon functionalization, the ASE wavelength (λ_{ASE}) also redshifts by around 2 nm, from 577 to 579 nm.

Graphs of the output intensity as a function of the pump intensity are displayed in Figure 3b. These are useful to determine the ASE threshold, i.e., the pump intensity at which the output intensity increases abruptly. For the 10:1 phenyl-functionalized and the nonfunctionalized films (only data for the former are displayed, since they are similar), no spectral narrowing indicative of the presence of ASE was observed. The threshold decreases with increasing degree of phenyl functionalization. The lowest threshold (around 8 kW cm^{-2}) was obtained for the film with the highest degree of phenyl

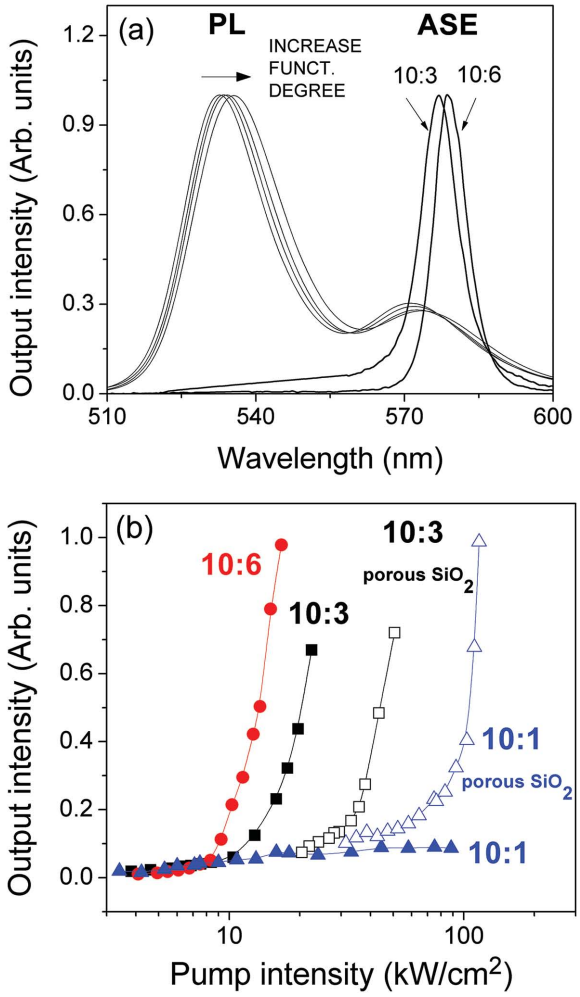

Figure 3. a) PL spectra of PDI-O-doped mesostructured silica films with different degrees of functionalization deposited over fused silica substrates (curves from left to right correspond to 10:0, 10:1, 10:3, and 10:6 phenyl-functionalized samples) and ASE spectra for the films with 10:3 and 10:6 phenyl functionalization; b) output intensity versus pump intensity for these films (full symbols) and for similar ones with intercalated porous SiO_2 layer between mesostructured film and fused silica substrate (open symbols). Lines are guides to the eye.

functionalization (10:6). This threshold value is only slightly higher than the minimum value obtained to date with PDI-O-doped PS films (3 kW cm^{-2}). This is a very important result, taking into account the lower quality of mesostructured silica waveguides in comparison to PS waveguides. It is also remarkable the fact that these relatively low thresholds have been achieved by waveguides simply consisting of the active films deposited over fused silica substrates.

As discussed in detail in Section 2.3, waveguiding is possible in these structures thanks to the increase in the silica refractive index achieved by its phenyl functionalization. In previously published work related to laser activity from dye-doped mesostructured materials, the lack of contrast between n_f and n_s required the intercalation of a low-n layer between film and substrate in refs. [5b,5d]. Such a strategy resulted in ASE, though has several drawbacks. First, the structure is more complicated, and second and more important, such low-n layers are generally unstable and their optical quality and uniformity is poor, thus limiting ASE performance.

To further demonstrate the benefits of the simple waveguide structures used here, we prepared several samples with a low-n porous silica film (n = 1.2) intercalated between the mesostructured film and the fused silica substrate. In this case, ASE could be obtained from samples based on nonfunctionalized and 10:1 phenyl-functionalized silica films, although their thresholds are very large (see Figure 3b). We also prepared films of 10:3 phenyl-functionalized silica with an intercalated porous silica layer. In spite of its better waveguide mode confinement (see the discussion in Section 2.3), its threshold is larger than the one obtained without the low-n layer. This is attributed to the poor quality of the porous silica layer, which would increase the losses of the waveguide structure. The poor quality and instability of the porous silica film are also responsible for the lack of reproducibility found in apparently similar samples. For example, we found differences on the threshold values of up to an order of magnitude for samples with nonfunctionalized and 10:1 phenyl-functionalized silica. This reinforces the advantage of the herein reported simple structures based on phenyl-functionalized silica for which no such low-n layers are needed.

2.3. Effect of Functionalization on the Waveguide Properties

The waveguiding properties have been investigated experimentally (by the m-line technique at a wavelength λ = 578 nm; see the Experimental Section) for all samples with and without intercalation of a low-n index layer. The experimental effective indexes (n_{eff}) associated with the transverse electric (TE) modes propagating in the structures are shown in **Figure 4** (right axis). These values were then used to calculate the refractive index of the active films (n_f) for each case (left axis; see the Experimental Section). In particular, an n_f value of 1.46 was obtained for the nonfunctionalized mesostructured silica film. In other publications, n_f values of 1.43 and of 1.4–1.5 have been reported for SiO_2/P123 films doped with Rh6G.[5d,e] These small differences in n for presumably the same materials are attributed to different proportions of TEOS and P123 and/or the wavelength at which n is determined. In the case of films deposited over fused silica (Figure 4a), no waveguide modes were observed in the nonfunctionalized film since its refractive index approximately matches that of fused silica (n_s = 1.46). For the 10:1 phenyl-functionalized film, n_f was slightly larger (i.e., 1.48), but the difference to the refractive index of the substrate was too small to allow waveguiding. In contrast, one TE mode (TE_0) propagates in the 10:3 and 10:6 phenyl-functionalized silica films, thanks to their large enough refractive indexes of 1.49 and 1.50, respectively. Interestingly, the observed dependence trend of n_f versus the functionalization degree could be used to infer n_f at functionalization ratios higher than those prepared in this work. However, as explained above, phenyl functionalization ratios higher than 10:6 lead to a decrease of the optical film quality and to a lack of mesostructural order. So, according to our data, the maximum expected refractive index change (Δn) while preserving film optical quality and mesostructural order would be $\Delta n \approx 0.04$. For films deposited over

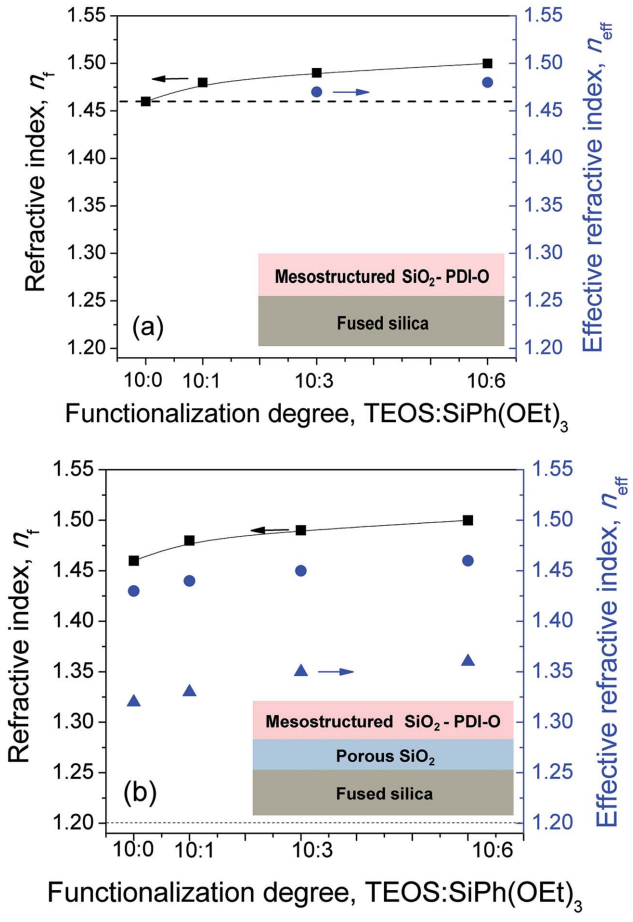

Figure 4. Experimental effective refractive index of TE modes (n_{eff}, right axis, circles and triangles for TE_0 and TE_1, respectively) and refractive index (n_f, left axis, lines are guides to the eye), calculated from these n_{eff} values as a function of silica functionalization degree, for mesostructured films deposited over fused silica plates a) without and b) with intercalated porous SiO_2 layer. The refractive index of the substrate, fused silica in (a) and mesoporous SiO_2 in (b), is indicated with a dashed line. The functionalization degree is expressed as the proportions of TEOS and $SiPh(OEt)_3$.

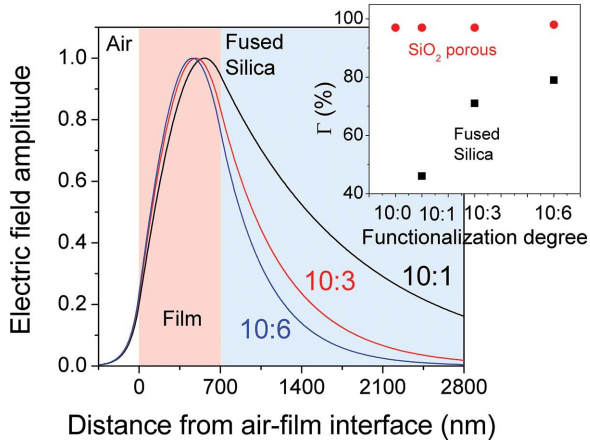

Figure 5. Electric field amplitude of the TE_0 waveguide mode, normalized to its maximum value, as a function of the distance from the air–film interface for functionalized mesostructured silica films deposited over fused silica. The calculated waveguide mode confinement parameter (Γ) is represented in the inset (squares), where results for similar waveguides but with a porous SiO_2 layer intercalated between the silica film and the fused silica have also been included (circles).

porous SiO_2 layers, previously spin-coated over fused silica plates (Figure 4b), two TE modes were observed in all cases due to the significant refractive index difference between film and the porous SiO_2 substrate (1.46–1.50 vs 1.20).

For asymmetric waveguides, such as the ones prepared here, there is a condition that needs to be fulfilled in order to get the light guided within the film, besides the one just discussed of having $n_f > n_s$: Film thickness (h_f) should be larger than a certain value, denoted as the cut-off thickness for the propagation of one mode ($h_{cut\text{-}off}$). The calculated $h_{cut\text{-}off}$ values for the TE_0 mode at λ_{ASE} are 511, 401, and 337 nm, for the films with functionalization degrees of 10:1, 10:3, and 10:6, respectively (see the Experimental Section for details). Importantly, to obtain low ASE thresholds and high ASE efficiencies, h_f should be sufficiently high to ensure a high-mode confinement and consequently low propagation losses (typically around 200 nm above $h_{cut\text{-}off}$), but not too large as to avoid the presence of higher order modes.[11b] Based on these requirements, we chose $h_f \approx 700$ nm for our films, similar for all of them (despite their different $h_{cut\text{-}off}$) to facilitate a proper analysis of the influence of the refractive index change due to the silica functionalization.

Waveguide mode confinement was studied for the films deposited directly over fused silica plates and is illustrated in **Figure 5**. This figure shows the electric field profile of the optical beam propagating in the waveguide structure for various degrees of phenyl functionalization. The confinement of the waveguide mode increases with the degree of functionalization, as a consequence of the increasing refractive index difference between film and substrate. The confinement factor parameter Γ, a quantitative measure for the degree of mode confinement, is plotted in the inset of Figure 5 (see the Experimental Section for calculation details). Results for mesostructured silica films deposited over the porous SiO_2 layers have also been included in the inset. As expected, a better mode confinement is achieved when using the lower refractive index porous SiO_2. However, as discussed in previous section, this advantage is overcompensated by larger ASE thresholds, low ASE reproducibilities due to the poor optical quality of the porous SiO_2 layers, and the presence of higher order modes increasing waveguide losses.

2.4. Influences of Functionalization on the Structures and Distributions of PDI-O within the Mesostructured Materials

Understanding molecular level interactions and distributions of the PDI-O molecules within the mesostructured composites is important for understanding the macroscopic stimulated emission behavior. These interactions and distributions can be established by solid-state 2D NMR techniques that exploit dipole–dipole couplings to correlate the chemical shifts of molecularly proximate moieties. Specifically, these methods yield enhanced spectral or temporal resolution of ^1H and ^{13}C signals associated with the surfactant, silica, and/or PDI-O species. In particular, 2D $^{13}C\{^1H\}$ and $^{29}Si\{^1H\}$ HETCOR spectra differentiate among the different ^1H and ^{13}C or ^{29}Si moieties on

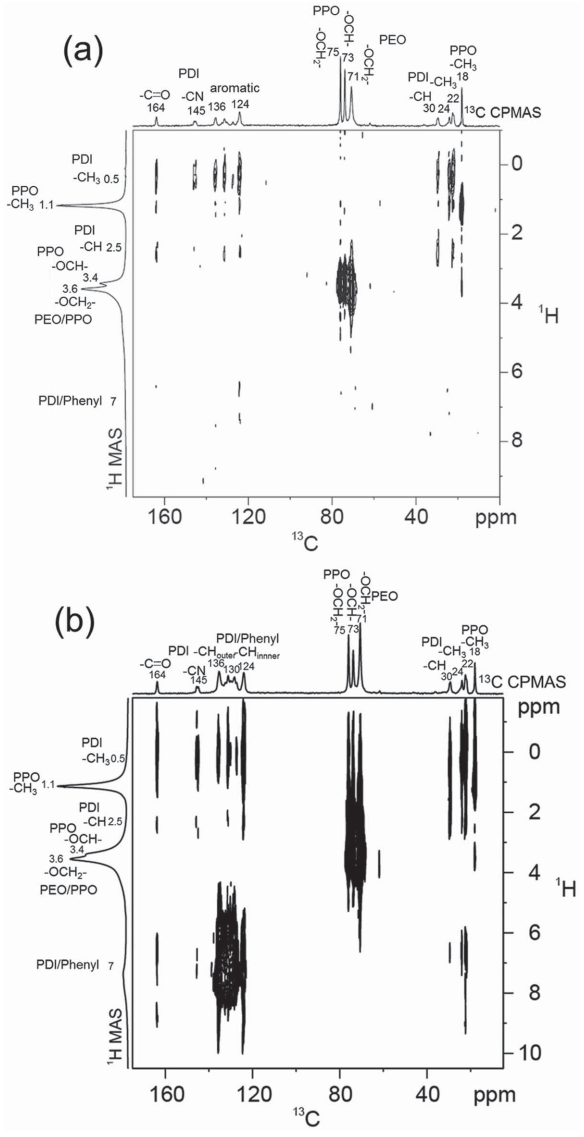

Figure 6. 2D $^{13}C\{^{1}H\}$ HETCOR NMR spectra acquired at room temperature and under MAS conditions of 12.5 kHz for mesostructured silica-P123-PDI (2%) composite either a) without or b) with functionalization by the addition of phenyl groups (10:3 ratio). Single-pulse 1D ^{1}H MAS and 1D $^{13}C\{^{1}H\}$ CP-MAS spectra are shown along the left vertical and top horizontal axes, respectively. Signals from the P123, PDI, and phenyl groups are observed with some overlap of phenyl signals with the PDI aromatic signals in (b). Ring current effects arising from intermolecular interactions between the P123 and the aromatic PDI moieties are observed in (b), indicating that the PDI is distributed throughout P123.

the basis of their isotropic chemical shifts. **Figure 6** shows 2D $^{13}C\{^{1}H\}$ heteronuclear correlation (HETCOR) spectra acquired at room temperature for mesostructured P123-silica (Figure 6a) and mesostructured P123-phenyl-functionalized silica (10:3 functionalization ratio, Figure 6b); both samples contained 2% PDI-O. Single-pulse 1D ^{1}H MAS and 1D $^{13}C\{^{1}H\}$ CP-MAS spectra are shown along the left vertical and top horizontal axes, respectively, to aid interpretation of the 2D HETCOR spectra. The integrated intensities of the 1D $^{13}C\{^{1}H\}$ CP-MAS spectrum are influenced by the relative populations and extents of ^{1}H–^{13}C dipolar coupling associated with the respective ^{13}C moieties, which depend on their intermolecular separation distances (≈1 nm) and molecular mobilities (>μs correlation times).[17] A number of well-resolved signals from the block copolymer and PDI-O are observed for both samples and are labeled in the $^{13}C\{^{1}H\}$ CP-MAS spectra. The strongest intensity correlations arise from proximities between ^{1}H and ^{13}C nuclei associated with the P123 structure-directing species. For example, the ^{1}H signal at 1.1 ppm is strongly correlated with the ^{13}C signal at 18 ppm associated with the —CH_3 groups of the poly(propyleneoxide) (PPO) blocks, while the ^{1}H signal at 3.4–3.6 ppm exhibits strong correlation with the ^{13}C signals at 71, 73, and 75 ppm associated with the —OCH_2— moieties of poly(ethyleneoxide) (PEO), and the —OCH_2— and —OCH— moieties of PPO, respectively. In addition to these strong intensity correlations among the P123 moieties, unambiguous correlations among the ^{1}H and ^{13}C moieties of the PDI-O are also observed, specifically between ^{13}C signals, at 22, 24, 30, 145, and 164 and ^{1}H signals ≈0 and 6.5 ppm. The two PDI —CH_3 ^{13}C signals at 22 and 24 ppm arise from some methyl groups hydrogen bonding to nearby nitrogen atoms.[6b]

The influence of the phenyl functionalization on the interactions and distributions of the PDI-O and the structure-directing P123 can also be established from intermolecular interactions in the HETCOR spectra. For example, in Figure 6a weak intermolecular intensity correlations are observed between ^{13}C signals at 164, 124, 24, and 22 ppm from the PDI dye species and the ^{1}H signal at 1.1 ppm from the PPO —CH_3 groups. In the spectrum of the phenyl-functionalized silica (Figure 6b), these same correlations are observed with more intensity; this additional intensity may be due to phenyl groups reducing the molecular mobility of the PDI-O molecules (and other species such as the P123), leading to enhanced polarization transfer between ^{13}C and ^{1}H moieties. Furthermore, additional intermolecular intensity correlations are observed between these PDI ^{13}C signals and ^{1}H signals at ≈0 and 7 ppm that arise from phenyl groups at the silica surface. Intermolecular intensity correlations observed in a $^{29}Si\{^{1}H\}$ HETCOR spectrum (Supporting Information, Figure S2) acquired for PDI-P123-phenyl-functionalized silica also indicate that P123 interacts strongly with and likely penetrates into the silica matrix, which may promote the incorporation of the PDI-O within the silica matrix as well. In addition, molecules with aromatic rings, such as the PDI-O, induce small, local fields that affect the isotropic chemical shifts of nearby moieties; these local fields arise from the effects of large static B_0 magnetic field on delocalized electrons in π-orbitals of the aromatic rings. While the ring-current effects of these small, local magnetic fields are generally small (up to several ppm), they can often be observed in the ^{1}H signals of nearby moieties.[18] In the case of the ^{1}H signals associated with P123 in the 2D HETCOR spectrum, broadening is observed in the ^{1}H dimension to lower frequencies (2.0–3.5 ppm ^{1}H) of the ^{13}C signals at 73 and 75 ppm from the —OCH— and —OCH_2— groups associated with PPO and at 71 ppm from the PEO —OCH_2— moieties (this region of the spectrum is enlarged in Figure S3 in the Supporting Information.) The fact that this broadening is present in both PEO and PPO moieties suggests that the PDI-O is distributed among both

the PEO and PPO blocks of the structure-directing surfactant species. In contrast, for the P123-silica-PDI sample without phenyl functionalization (Figure 6a), very minimal broadening is seen for the ^{1}H signals of the P123 moieties, suggesting that the PDI is mostly aggregated, rather than interacting strongly with the surfactant species. From the NMR analyses, it can be concluded that the PDI-O interacts with both the PEO and PPO blocks of the P123 surfactant species and that such dispersal is furthermore facilitated by phenyl functionalization in the silica framework.

3. Conclusions

Low thresholds for ASE are observed from simple waveguide structures consisting of mesostructured silica films doped with a PDI laser dye, deposited directly over fused silica substrates. This has been achieved by functionalizing the mesostructured silica network with phenyl groups, which leads to a sufficiently large increase in the refractive index of the active layer to enable efficient waveguiding and thus ASE at low thresholds with good reproducibility. This result is remarkable in the context of previous laser studies with mesostructured silica-based materials, in which a cladding layer of a low-refractive-index material (typically porous SiO_2) intercalated between the active film and the substrate was needed to obtain ASE, generally at higher threshold and poorer reproducibility. By forming a high-quality waveguide without the need for a separate low-refractive-index layer, significantly improved properties are obtained, with ASE thresholds as low as 8 kW cm^{-2}. These results are expected to be general for other laser dyes incorporated into host materials and open opportunities for simpler device configurations and improved performances.

4. Experimental Section

Materials: All chemicals were reagent-grade, purchased from commercial sources and used as received unless otherwise specified. PDI-O (M = 711 g mol^{-1}) was purchased from Phiton with a purity higher than 99.5%. TEOS, $SiPh(OEt)_3$, two structure-directing poly(ethylene glycol)-poly(propylene glycol)-poly(ethylene glycol) triblock copolymer surfactants (Pluronic P123, $EO_{20}PO_{70}EO_{20}$, M_n = 5750 g mol^{-1}, and Pluronic F127, $EO_{106}PO_{70}EO_{106}$, M_n = 12600 g mol^{-1}), tetrahydrofuran (THF), and anhydrous ethanol were purchased and used as received from Sigma Aldrich Chemicals.

Synthetic Procedures: In a typical synthesis of mesostructured silica, 0.414 g TEOS was hydrolyzed in a solution containing 0.162 mL HCl (0.07 M) and 1.053 mL THF at room temperature without stirring for 1 h. To prepare silica functionalized with phenyl groups, $SiPh(OEt)_3$ was added in various weight ratios. Separately, a solution containing 0.162 g P123 and 1.98 mL THF was prepared, which was then added to the TEOS solution. Finally, the PDI-O laser dye was added at percentages with respect to the solid mass between 0.5% and 3%. The final solution containing TEOS/P123/PDI-O was stirred for 1 h and deposited as 700 nm thick films by spin-coating over commercial fused silica plates or over mesoporous SiO_2 layers that had previously been spin-coated over fused silica plates.

The mesoporous SiO_2 was synthesized as follows: 1.353 g TEOS was hydrolyzed in a mixed solution containing 0.099 mL HCl (0.3 M), 0.495 mL H_2O, and 1.564 mL ethanol at room temperature. Then, 3.19 g of this solution was added to a second solution containing 0.3 g F127 and 2.37 mL ethanol. The mixture was stirred for 2 h at room temperature and deposited as thin films by spin-coating over fused silica plates. The films were dried at 25 °C for several days and then calcined at 500 °C in air for 8 h.

Optical Characterization: Standard PL and absorbance measurements of the active film were carried out in a Jasco FP-6500/6600 fluorimeter and in a Jasco V-650 spectrophotometer, respectively. The ASE properties of the active films were explored by optical excitation with a frequency-doubled Nd:YAG (YAG-yttrium aluminum garnet) laser (10 ns, 10 Hz) operating at 532 nm, close to the maximum absorbance of PDI-O. A cylindrical lens and an adjustable slit were used to shape the beam into a stripe of 3.5 × 0.5 mm^2. The stripe was placed at the edge of the film from where PL emission was detected with an Ocean Optics USB2000-UV-VIS fiber spectrometer with a resolution of 1.3 nm.

Refractive index and thickness of the mesostructured films (n_f and h_f, respectively) were determined by solving the propagation wave equation for the waveguide structure, assuming a substrate, either fused or porous silica, of infinite thickness. The n_{eff} values used in the calculation were determined by the *m*-line technique,[19] using a mercury lamp emitting at λ = 580 nm as light source. For films that did not support waveguide modes, n_f was determined by measuring the reflectivity of polarized light at various angles of incidence.[20] The confinement factor of the TE_0 mode (Γ), defined as the fraction of the electric field energy in the active film, was obtained from[19]

$$\Gamma = \frac{\int_0^{h_f} |E(x)|^2 \, dx}{\int_{-\infty}^{+\infty} |E(x)|^2 \, dx} \quad (1)$$

The minimum thickness needed to enable propagation of the TE_0 mode ($h_{cut\text{-}off}$) at wavelength λ can be calculated by[19]

$$h_{cut\text{-}off} = \frac{\lambda}{2\pi\sqrt{n_f^2 - n_s^2}} \tan^{-1}\left(\sqrt{\frac{n_s^2 - n_c^2}{n_f^2 - n_s^2}}\right) \quad (2)$$

where n_c is the refractive index of the cover layer (air in this case, n_c = 1).

X-Ray Scattering Characterization: Small-angle X-ray scattering (SAXS) patterns were acquired to establish the degree of mesostructural ordering in the silica films. These measurements were conducted with a XENOCS Genix 50W X-ray microsource with Cu K_α radiation (λ = 1.542 Å, voltage 50 keV, current 1 mA) and an MAR345 image plate area detector (located 1.4 m behind the sample) in a transmission geometry.

Solid-State NMR Characterization: Solid-state 2D $^{13}C\{^1H\}$ heteronuclear correlation NMR experiments were conducted at 11.7 tesla using a Bruker AVANCE II spectrometer operating at frequencies of 500.24 MHz for ^{1}H and 125.79 MHz for ^{13}C. The experiments were performed at room temperature under magic-angle-spinning (MAS) conditions using a 4 mm double-resonance variable-temperature Bruker MAS probehead. Cross-polarization (CP) was used to transfer magnetization from ^{1}H to ^{13}C nuclei by adiabatic passage through the Hartmann–Hahn condition.[21] Heteronuclear ^{1}H decoupling was applied during signal acquisition at a ^{1}H nutation frequency of 100 kHz by using the pulse sequence SPINAL-64.[22] Quadrature detection in the indirect ^{1}H dimension was achieved by using time-proportional-phase-incrementation (TPPI).[23] The 2D spectra were acquired by using a 1 s recycle delay and under MAS conditions of 12.5 kHz with a 2 ms CP contact time. Additionally, high-power ^{1}H–^{1}H homonuclear decoupling using the eDUMBO-1_{22} sequence was applied during the ^{1}H evolution time with a phase-modulated radio frequency pulse of constant amplitude (100 kHz).[24] In the indirect (^{1}H) dimension, a scaling factor of 0.6–0.65 was calibrated from separate 2D ^{1}H–^{1}H spin diffusion NMR experiments. Contour levels shown in the 2D NMR spectrum correspond to 5%, 10%, 25%, 40%, 55%, 70%, and 85% of the maximum signal intensity. ^{13}C and ^{1}H chemical shifts were referenced to neat tetramethylsilane (TMS, 0 ppm), using tetrakis-methylsilane as an external secondary reference (^{13}C and ^{1}H chemical shifts of 3.52 and 0.25 ppm relative to TMS, respectively).[25]

Supporting Information

Supporting Information is available from the Wiley Online Library or from the author.

Acknowledgements

The authors thank support from the Spanish Government through the "Ministerio de Economía y Competitividad" (MINECO) and the European Community (FEDER) through grant nos. MAT2008–06648-C02 and MAT2011–28167-C02. M.G.R. has been supported by a CSIC fellowship within the program JAE. M.A.D.G. acknowledges funding received from the "Ministerio de Educación y Ciencia, MEC" (reference no. PR2009–0456) to perform a research stay at UCSB to initiate the collaboration between the two teams contributing to this work. M.J.N.J. acknowledges financial support from the Alexander von Humboldt-Foundation through a Feodor Lynen Research Fellowship. The NMR experiments were conducted in the Central Facilities of the UCSB Materials Research Laboratory supported by the MRSEC program of the U.S. NSF under award no. DMR-1121053. The work at UCSB was supported by the USARO through the Institute for Collaborative Biotechnologies through W911NF-09-D-0001. The content of the information does not necessarily reflect the position or the policy of the Government, and no official endorsement should be inferred.

Received: May 31, 2015
Revised: July 3, 2015
Published online: August 6, 2015

[1] J. Clark, G. Lanzani, *Nat. Photonics* **2010**, *4*, 438.
[2] M. Lu, S. S. Choi, C. J. Wagner, J. G. Eden, B. T. Cunningham, *Appl. Phys. Lett.* **2008**, *92*, 261502.
[3] M. B. Christiansen, J. M. Lopacinska, M. H. Jakobsen, N. A. Mortensen, M. Dufva, A. Kristensen, *Opt. Express* **2009**, *17*, 2722.
[4] a) I. D. W. Samuel, G. A. Turnbull, *Chem. Rev.* **2007**, *107*, 1272; b) S. Chenais, S. Forget, *Polym. Int.* **2011**, *61*, 390; c) C. Grivas, M. Pollnau, *Laser Photonics Rev.* **2012**, *6*, 419; d) E. R. Martins, Y. Wang, A. L. Kanibolotsky, P. J. Skabara, G. A. Turnbull, I. D. W. Samuel, *Adv. Opt. Mater.* **2013**, *1*, 563; e) J. Casado, V. Hernández, J. T. López Navarrete, M. Algarra, D. A. da Silva Filho, S. Yamaguchi, R. Rondão, J. S. Seixas de Melo, V. Navarro-Fuster, P. G. Boj, M. A. Díaz-García, *Adv. Opt. Mater.* **2013**, *1*, 588; f) H. Fang, R. Ding, S. Lu, X. Zhang, J. Feng, Q. Chen, H. Sun, *J. Mater. Chem.* **2012**, *22*, 24139.
[5] a) F. Marlow, M. D. McGehee, D. Y. Zhao, B. F. Chmelka, G. D. Stucky, *Adv. Mater.* **1999**, *11*, 632; b) P. D. Yang, G. Wirnsberger, H. C. Huang, S. R. Cordero, M. D. McGehee, B. Scott, T. Deng, G. M. Whitesides, B. F. Chmelka, S. K. Buratto, G. D. Stucky, *Science* **2000**, *287*, 465; c) C. W. Wu, M. Kuwabara, *Sci. Technol. Adv. Mater.* **2003**, *4*, 593; d) B. J. Scott, G. Wirnsberger, M. D. McGehee, B. F. Chmelka, G. D. Stucky, *Adv. Mater.* **2001**, *13*, 1231; e) R. Vogel, P. Meredith, I. Kartini, M. Harvey, J. D. Riches, A. Bishop, N. Heckenberg, M. Trau, H. Rubinsztein-Dunlop, *Chem. Phys. Chem.* **2003**, *4*, 595.
[6] a) E. M. Calzado, J. M. Villalvilla, P. G. Boj, J. A. Quintana, R. Gómez, J. L. Segura, M. A. Díaz-García, *J. Phys. Chem. C* **2007**, *111*, 13595; b) M. G. Ramírez, M. Morales-Vidal, V. Navarro-Fuster, P. G. Boj, J. A. Quintana, J. M. Villalvilla, A. Retolaza, S. Merino, M. A. Díaz-García, *J. Mater. Chem. C* **2013**, *1*, 1182; c) M. G. Ramírez, S. Pla, P. G. Boj, J. M. Villalvilla, J. A. Quintana, M. A. Díaz-García, F. Fernández-Lázaro, A. Sastre-Santos, *Adv. Opt. Mater.* **2013**, *1*, 933.
[7] a) W. C. Molenkamp, M. Watanabe, H. Miyata, S. H. Tolbert, *J. Am. Chem. Soc.* **2004**, *126*, 4476; b) T. Q. Nguyen, J. J. Wu, V. Doan, B. J. Schwartz, S. H. Tolbert, *Science* **2000**, *288*, 652; c) J. J. Wu, A. F. Gross, S. H. Tolbert, *J. Phys. Chem. B* **1999**, *103*, 2374; d) W. Xu, H. Q. Guo, D. L. Akins, *J. Phys. Chem. B* **2001**, *105*, 7686; e) J. W. Long, B. Dunn, D. R. Rolison, H. S. White, *Chem. Rev.* **2004**, *104*, 4463; f) S. Neyshtadt, J. P. Jahnke, R. J. Messinger, A. Rawal, D. Huppert, B. F. Chmelka, G. L. Frey, *J. Amer. Chem. Soc.* **2011**, *133*, 10119.
[8] J. D. Epping, B. F. Chmelka, *Curr. Opin. Colloid Interface Sci.* **2006**, *11*, 81.
[9] a) N. A. Melosh, P. Davidson, B. F. Chmelka, *J. Am. Chem. Soc.* **2000**, *122*, 823; b) N. A. Melosh, P. Davidson, P. Feng, D. J. Pine, B. F. Chmelka, *J. Am. Chem. Soc.* **2001**, *123*, 1240; c) N. A. Melosh, P. Lipic, F. S. Bates, F. Wudl, G. D. Stucky, G. H. Fredrickson, B. F. Chmelka, *Macromolecules* **1999**, *32*, 4332.
[10] C. A. Steinbeck, M. Ernst, B. H. Meier, B. F. Chmelka, *J. Phys. Chem. C* **2008**, *112*, 2565.
[11] a) E. M. Calzado, J. M. Villalvilla, P. G. Boj, J. A. Quintana, M. A. Díaz-García, *J. Appl. Phys.* **2005**, *97*, 093103; b) E. M. Calzado, M. G. Ramírez, P. G. Boj, M. A. Díaz García, *Appl. Opt.* **2012**, *51*, 3287; c) M. Anni, A. Perulli, G. Monti, *J. Appl. Phys.* **2012**, *111*, 093109.
[12] a) F. Lahoz, C. J. Oton, N. Capuj, M. Ferrer-González, S. Cheylan, D. Navarro-Urrios, *Opt. Express* **2009**, *17*, 16766; b) M. G. Ramírez, J. A. Quintana, J. M. Villalvilla, P. G. Boj, A. Retolaza, S. Merino, M. A. Díaz-García, *J. Appl. Phys.* **2013**, *114*, 033107.
[13] M. G. Ramirez, P. G. Boj, V. Navarro-Fuster, I. Vragovic, J. M. Villalvilla, I. Alonso, V. Trabadelo, S. Merino, M. A. Díaz-García, *Opt. Express* **2011**, *19*, 22443.
[14] a) A. Costela, I. García-Moreno, R. Sastre, *Phys. Chem. Chem. Phys.* **2003**, *5*, 4745; b) Y. Yang, M. Wang, G. Qian, Z. Wang, X. Fan, *Opt. Mater.* **2004**, *24*, 621; c) A. K. Sheridan, A. R. Buckley, A. M. Fox, A. Bacher, D. D. C. Bradley, I. D. W. Samuel, *J. Appl. Phys.* **2002**, *92*, 6367; d) V. Navarro-Fuster, E. M. Calzado, P. G. Boj, J. A. Quintana, J. M. Villalvilla, M. A. Díaz-García, V. Trabadelo, A. Juarros, A. Retolaza, S. Merino, *Appl. Phys. Lett.* **2010**, *97*, 171104.
[15] a) W. Herbst, K. Hunger, *Industrial Organic Pigments: Production, Properties, Applications*, 2nd ed., Wiley-VCH, Weinheim, Germany **1997**; b) H. Langhals, *Heterocycles* **1995**, *40*, 477.
[16] D. Y. Zhao, J. L. Feng, Q. S. Huo, N. Melosh, G. H. Fredrickson, B. F. Chmelka, G. D. Stucky, *Science* **1998**, *279*, 548.
[17] K. Schmidt-Rohr, H. W. Spiess, *Multidimensional Solid-State NMR and Polymers*, Academic Press, San Diego, CA, USA **1994**.
[18] C. A. Steinbeck, N. Hedin, B. F. Chmelka, *Langmuir* **2004**, *20*, 10399.
[19] A. Boudrioua, *Photonic Waveguides: Theory and Applications*, Wiley, London, UK **2009**.
[20] T. Kihara, K. Yokomori, *Appl. Opt.* **1990**, *29*, 5069.
[21] S. Hediger, B. H. Meier, N. D. Kurur, G. Bodenhausen, R. R. Ernst, *Chem. Phys. Lett.* **1994**, *223*, 283.
[22] B. M. Fung, A. K. Khitrin, K. Ermolaev, *J. Magn. Reson.* **2000**, *142*, 97.
[23] D. Marion, K. Wuthrich, *Biochem. Biophys. Res. Commun.* **1983**, *113*, 967.
[24] B. Elena, G. de Paepe, L. Emsley, *Chem. Phys. Lett.* **2004**, *398*, 532.
[25] S. Hayashi, K. Hayamizu, *Bull. Chem. Soc. Jpn.* **1991**, *64*, 685.

ADVANCED OPTICAL MATERIALS

Supporting Information

for *Advanced Optical Materials*, DOI: 10.1002/adom. 201500297

Improved Amplified Spontaneous Emission of Dye-Doped Functionalized Mesostructured Silica Waveguide Films

Manuel G. Ramírez, Justin P. Jahnke, Matthias J. N. Junk, José M. Villalvilla, Pedro G. Boj, José A. Quintana, Eva M. Calzado, Bradley F. Chmelka, and María A. Díaz-García**

Supporting Information

Improved amplified spontaneous emission of dye-doped functionalized mesostructured silica waveguide films

Manuel G. Ramírez, Justin P. Jahnk, Matthias J. N. Junk, José M. Villalvilla, Pedro G. Boj, José A. Quintana, Eva M. Calzado, Bradley F. Chmelka and María A. Díaz-García**

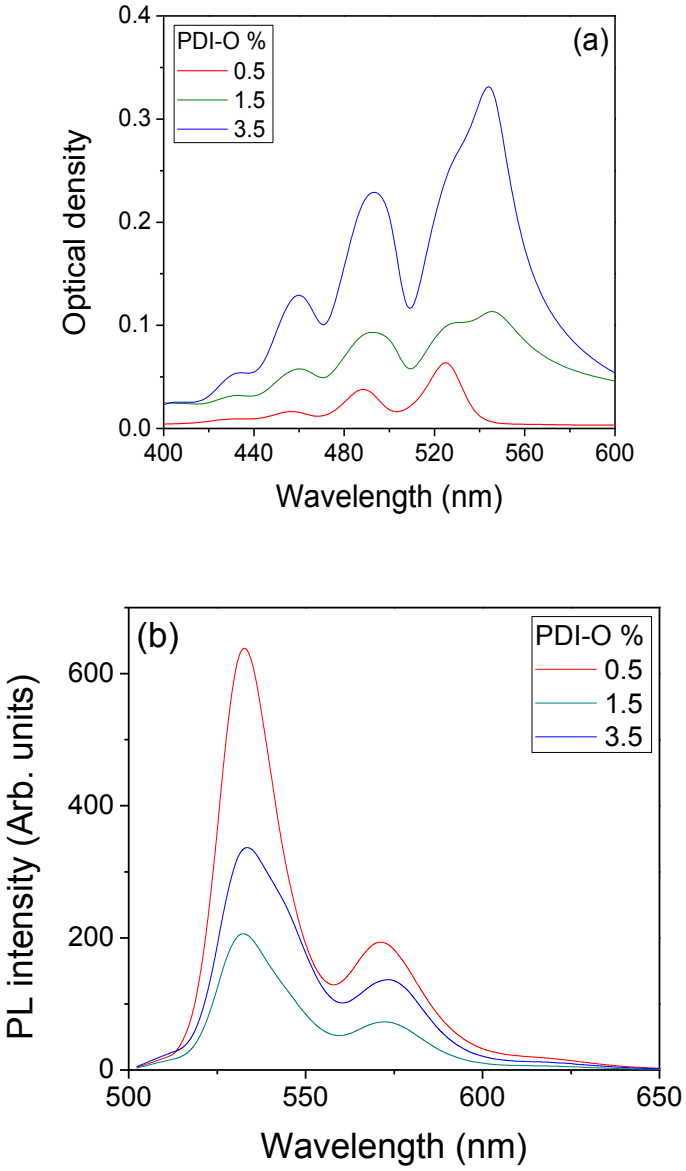

Figure S1: (a) Optical absorption and (b) PL spectra of mesostructured silica films doped with various amounts of PDI-O.

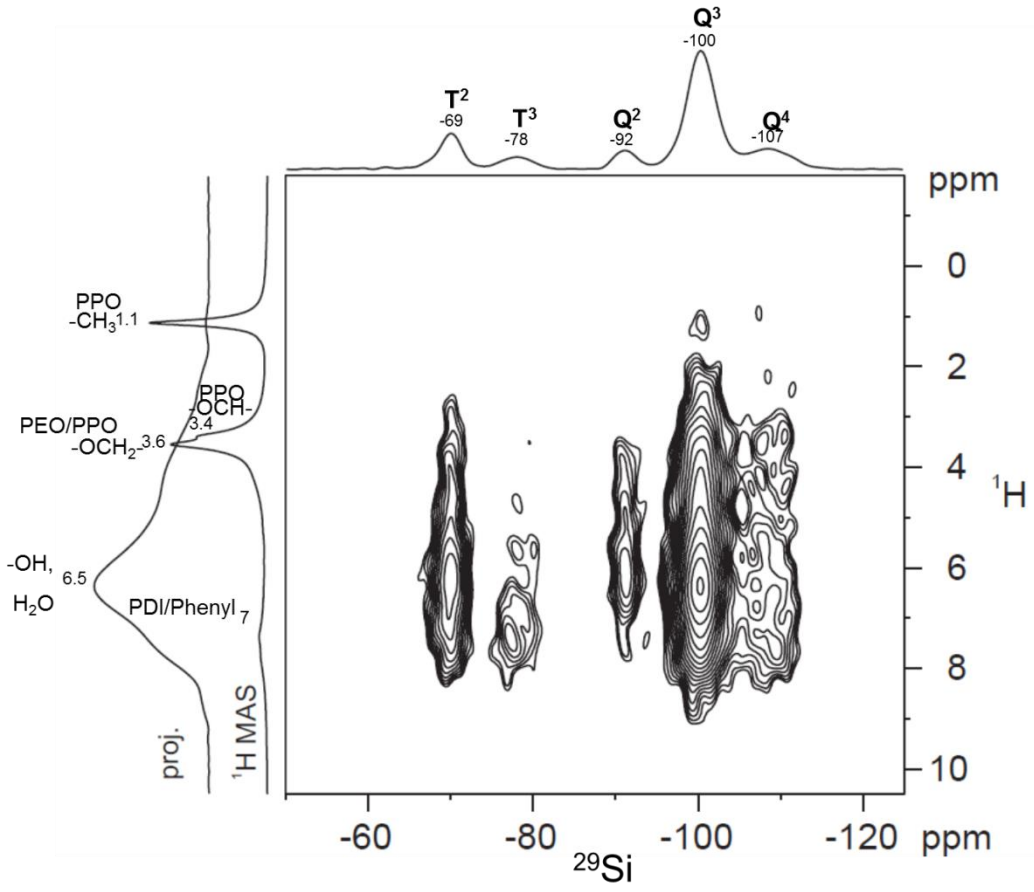

Figure S2: A 2D $^{29}Si\{^{1}H\}$ HETCOR spectrum acquired at room temperature for the mesostructured P123-phenyl functionalized silica containing 2 % PDI-O. 1D single-pulse ^{1}H MAS and 1D $^{29}Si\{^{1}H\}$ CP-MAS spectra are shown along the left vertical and top horizontal axes, respectively. A projection of the ^{1}H correlated signal intensity of the 2D spectrum is shown along the left vertical axis. The high intensity of the T^2 and Q^3 species relative to the fully cross-linked Q^4 and T^3 moieties suggests an incomplete cross-linking of the silica framework. All silicon species have strong intensity correlations with a broad ^{1}H signal ca. 6.5 ppm that is due to surface hydroxyls, bound water, and the silica phenyl groups. Many of the silicon moieties have intensity correlations in the regions of the ^{1}H spectrum where PEO and PPO moieties resonate, and, suggestively, a weak correlation is observed between ^{1}H signal at 1 ppm and the Q^3 silicon signal. This ^{1}H signal likely arises from the $-CH_3$ moieties of the PPO and suggests that the block copolymer is partially penetrating into the SiO_2 matrix, which may promote the incorporation of the PDI within the silica walls as well.

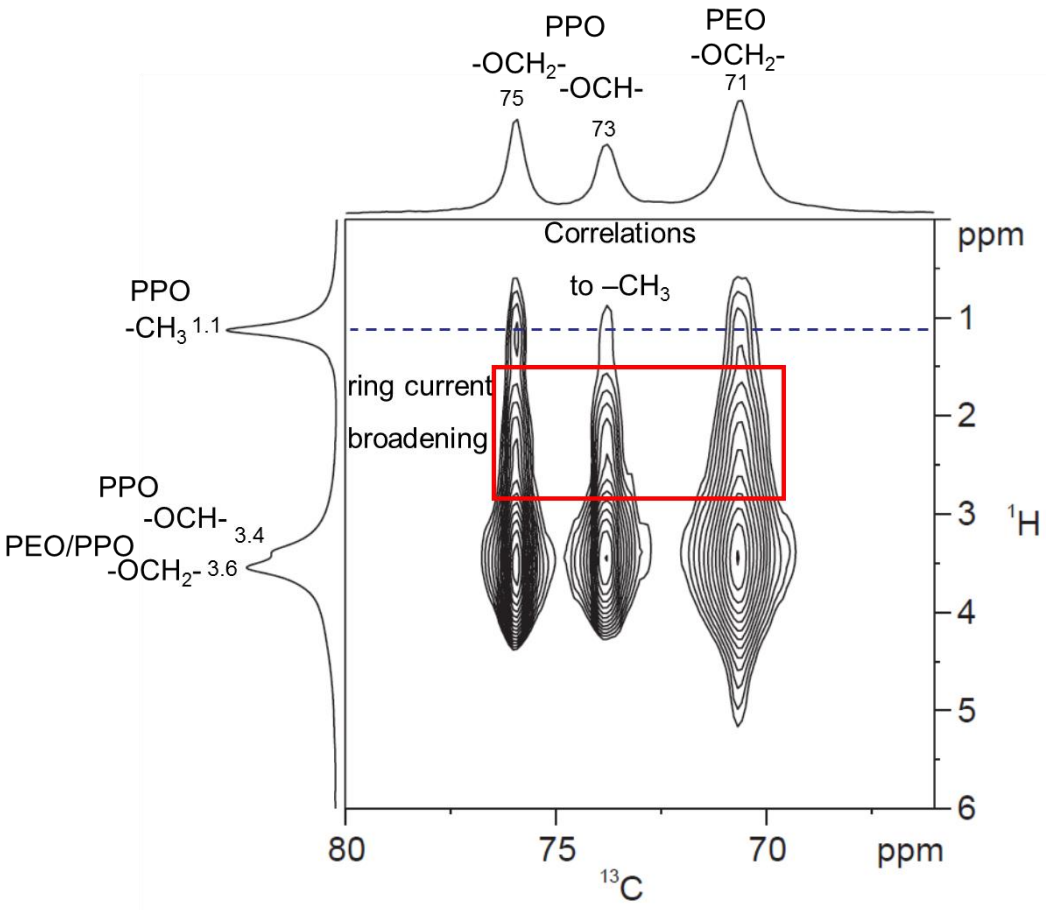

Figure S3: Expansion focusing on the –OCH_2–/–OCH– region of the 2D $^{13}C\{^1H\}$ HETCOR NMR spectrum shown in Figure 6(b). 1D single-pulse ^1H MAS and $^{13}C\{^1H\}$ CP-MAS spectra are shown along the left vertical and top horizontal axes, respectively, of the 2D spectrum. Asymmetric broadening to lower ppm is observed for all three correlations that is clearly distinct from the correlations to the P123 methyl group. This broadening is indicative of ring-current effects arising from P123 ^1H moieties being situated above or below the conjugated ring system of the PDI.